https://doi.org/10.5194/egusphere-2026-6214
Preprint. Discussion started: 10 November 2026
© Author(s) 2026. CC BY 4.0 License.

Rapid Deglacial Response of the Laurentide Ice Sheet during the Allerød Warm Interval Through the High Peak Wilderness of the Adirondack Mountains, New York, USA

Kelsey Barker[1], Aaron M. Barth[1], Joshua K. Cuzzone[2], Alan Hidy[3]
[1]Department of Geology, Rowan University, Glassboro, NJ, USA
[2]Joint Institute for Regional Earth System Science and Engineering, University of California, Los Angeles, CA, USA
[3]Center for Accelerator Mass Spectrometry, Lawrence Livermore National Laboratory, Livermore, CA, USA

Correspondence to: Kelsey Barker (barkerk1@rowan.edu)

Abstract. The Laurentide Ice Sheet (LIS) was the largest ice mass by volume during the last glacial cycle, containing approximately 75–85 m of global sea-level equivalent, and representing a major component of the climate system. Constraining the timing of LIS deglaciation is critical for evaluating its contributions to sea-level rise, climate variability, and ice-climate feedback. The Adirondack Mountains of New York (ADK) represent a topographically complex and previously under sampled region of the northeastern United States. Because this ~24,000 km^2 region represents a more interior component of the entire LIS, it provides an opportunity to investigate both the timing and mechanisms of interior ice-retreat following the Last Glacial Maximum. Here we present ^{36}Cl surface exposure ages from the High Peaks Wilderness region of the Adirondack Mountains, integrated with high-resolution transient ice-sheet model simulations to refine the timing and pattern of ice-sheet retreat through the mountainous terrain. Results suggest complete exposure of the region by 13.5 ± 0.6 ka (2σ), with modelled deglaciation occurring over an approximately 500-year interval, consistent with minimum-limiting radiocarbon ages indicating biotic reoccupation by ~13 cal ka. This updated chronology is younger than previous estimates for deglaciation across the northeastern United States, indicating later exposure during the Allerød warm interval (~14.2 to 13.0 ka). Our reconstructed ice-retreat chronology agrees with the ice-sheet modelling, which shows rapid thinning beginning at ~13.5–13.0 ka but delayed exposure of the High Peaks until the later Allerød. Together, these results suggest that Laurentide retreat through the Adirondacks lagged the onset of Bølling–Allerød warming before proceeding rapidly across the region.

1 Introduction

The Last Glacial Maximum (LGM), occurring between 26.5 and 19.5 ka (Clark et al., 2009), was characterized by the maximum extent of the Laurentide Ice Sheet (LIS), which represented the largest individual ice-sheet contribution to global sea-level equivalent at the time (Clark & Mix, 2002). The presence of the LIS had a substantial influence on the regional and global climate system by altering atmospheric circulation and precipitation patterns (Lora & Ibarra, 2019), and by modifying North Atlantic circulation and associated heat transport through deglacial meltwater discharge (Clark et al., 2001, Licciardi

https://doi.org/10.5194/egusphere-2026-6214
Preprint. Discussion started: 10 November 2026
© Author(s) 2026. CC BY 4.0 License.

et al., 1999). Resolving how the LIS responded to deglacial climate change therefore requires well-constrained records of the timing and pattern of ice-margin retreat across different sectors of the ice sheet. Across the northeastern United States, the timing and pattern of LIS retreat have been constrained using the abundance of preserved glacial landforms and deposits, together with a range of geochronometers including varve chronologies, (Ridge et al., 2012), basal radiocarbon (Dyke, 2004; Dalton et al., 2020), and *in situ* terrestrial cosmogenic nuclide (TCN) exposure dating (Balco & Schaefer, 2006; Balter-Kennedy et al., 2024; Bromley et al., 2015; Corbett et al., 2017; Thompson et al., 2017). However, the Adirondack Mountains of New York (ADK) (Fig. 1) remain underrepresented in regional geochronologic reconstructions of LIS retreat. The ADK was fully covered by the LIS at the LGM (Fairchild, 1913), and re-exposed during the subsequent deglaciation. Ice retreat through this topographically complex region altered major meltwater-routing pathways during deglacial flooding events (Franzi et al., 2026; Rayburn, 2007), contributing to changes in freshwater delivery to the North Atlantic with potential implications for Atlantic Meridional Overturning Circulation (AMOC) and associated heat transport (Clark et al., 2002; Licciardi et al., 1999). Improved constraints on the timing of LIS retreat through the ADK are therefore essential to understanding the response of the LIS to deglacial climate change, and for constraining the sensitivity and timescales of large ice sheet responses to abrupt warming.

https://doi.org/10.5194/egusphere-2026-6214
Preprint. Discussion started: 10 November 2026
© Author(s) 2026. CC BY 4.0 License.

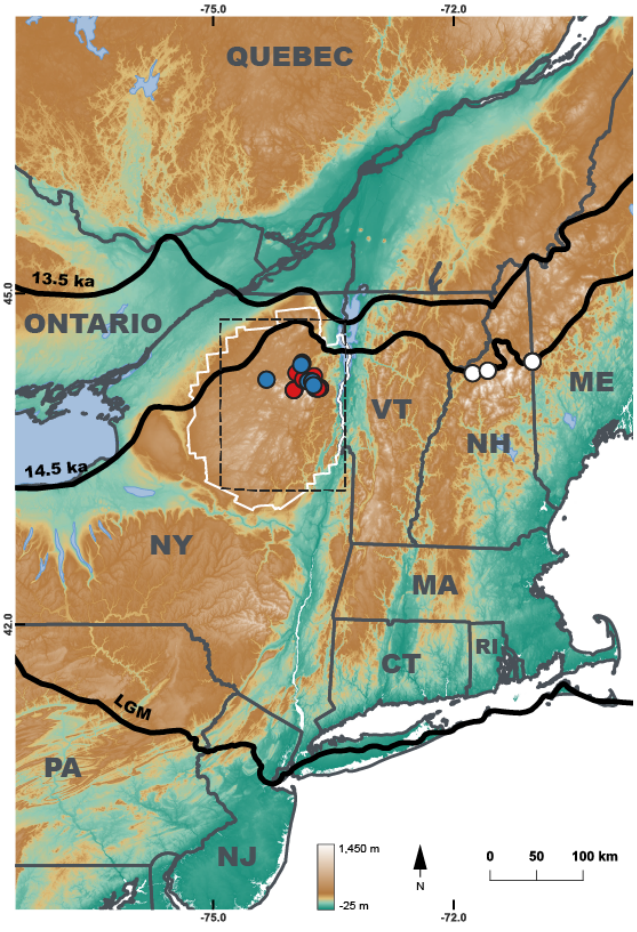


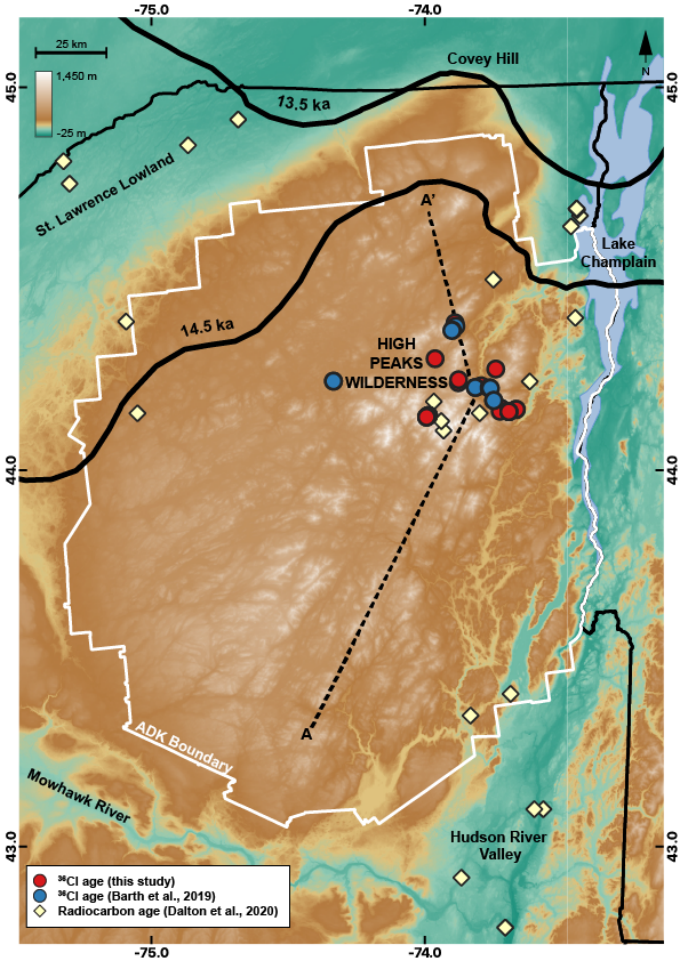
Figure 1: Regional map of the northeast United States. Bold black lines indicate ice margin positions of the Laurentide Ice Sheet taken from Dalton et al. (2020). Last Glacial Maximum extent indicated by the LGM margin. White line shows the boundary of the Adirondack Park. Symbols indicate the location of surface exposure ages from this study (blue), Barth et al., 2020 (red), and Bromley et al., 2015 (white). The dashed black line shows the model domain used in this study. Base image elevation generated using 10 m spatial data provided by the New York State Office of Information Technology Services.

Previous studies have attempted to constrain the timing and/or mechanisms associated with LIS retreat from the Adirondack region during the last deglacial climate transition (Barth et al., 2019; Davis, 1999; Franzi et al., 2016; Jackson, 1989; Porreca et al. 2018), documenting substantial ice-volume loss and evidence for rapid regional thinning (Barth et al., 2019) during the mid-deglacial (~15-13 ka). The surrounding lowlands of the Adirondack Mountains, including the Champlain Valley, experienced higher ice-flow velocities than the topographically complex terrain of the Adirondack Park (Cuzzone et al., 2025). The variable topography of the Adirondacks likely influenced local ice dynamics and may help explain why deglaciation there occurred later than in surrounding regions (Franzi et al., 2016). Additionally, recent ice-sheet modeling indicates that the LIS was cold-based across much of the ADK at the LGM, which would have limited basal sliding and

https://doi.org/10.5194/egusphere-2026-6214
Preprint. Discussion started: 10 November 2026
© Author(s) 2026. CC BY 4.0 License.

contributed to relatively sluggish ice flow through the region (Cuzzone et al., 2025). Despite these advances in our understanding of regional ice dynamics and deglacial behavior, the timing and rate of LIS retreat across the Adirondack region remain poorly constrained, with limited geochronologic data from within the park (Fig. 2). It is therefore important to expand the coverage of geochronologic data for this region, which represents a more interior sector of the southeastern LIS.

Here we present 12 new ^{36}Cl exposure ages that expand the existing TCN record within the High Peak Wilderness Region (Fig. 2). These new data increase the spatial and elevational coverage of TCN ages across the region, improving constraints on current reconstructions of LIS thinning and retreat. We pair these exposure ages with new ice sheet model simulations of deglacial LIS retreat across this region to investigate the physical mechanisms involved in the ice retreat. These new findings provide support to rapid LIS retreat through the High Peaks Wilderness, (Barth et al., 2019) while indicating later deglaciation than previously assumed.



https://doi.org/10.5194/egusphere-2026-6214
Preprint. Discussion started: 10 November 2026
© Author(s) 2026. CC BY 4.0 License.

Figure 2: Map of the Adirondack Mountains. Bold black lines indicate ice margin positions of the Laurentide Ice Sheet taken from Dalton et al. (2020). White line shows the boundary of the Adirondack Park (ADK). Circles indicate the location of surface exposure ages from this study (blue) and Barth et al., 2020 (red). Yellow diamonds are the locations of radiocarbon ages recalibrated in Dalton et al., 2020. Dashed line A-A' marks the location of our transient model simulation through the Adirondacks (see Figure 4). Base image elevation generated using 10 m spatial data provided by the New York State Office of Information Technology Services.

2 Geologic Background

The Adirondack Mountains occupy roughly 24,000 km^2 of northern New York State and form a broad dome-like structure composed primarily of high-grade metamorphic rocks of the Grenville Structural Province (Fig.1; Isachsen & Fisher, 1970). The region has experienced prolonged uplift and erosion, producing high topographic relief characterized by numerous peaks, composed primarily of anorthosite (Isachsen, 1981), which exceed 1,600 m elevation and valleys ~400–500 m asl. During the Pleistocene glacial cycles, the Adirondacks were repeatedly overridden by advances and retreats of the LIS which modified the landscape (Fairchild, 1913). At the LGM, the region was fully covered by the LIS and was re-exposed during the subsequent deglaciation, leaving behind glacial striations, erratic boulders, meltwater channels, and extensive outwash deposits that record its former presence (Franzi et al., 2016). Numerous proglacial lakes surrounded the region, including Glacial Lakes Iroquois and Abenaki, which were fed by meltwater from the receding LIS (Franzi et al., 2025). The St. Lawrence and Lake Champlain Lowlands served as major conduits for ice flow and meltwater drainage (Licciardi et al., 1999; Rayburn et al., 2007), while strath terraces in the Mohawk River Valley features record periods of meltwater drainage to the Hudson River during deglaciation (Porreca et al., 2018; Stanford, 2010).

3 Methods

3.1 ^{36}Cl surface exposure dating

Here we apply *in situ* TCN exposure dating methods to constrain the timing of LIS retreat from the Adirondack Mountains of New York. All collected samples are composed of feldspar- and pyroxene-rich anorthosite and lacking quartz, we therefore employ ^{36}Cl exposure dating methods in lieu of ^{10}Be. Advances in sample preparation and mineral separation now allow for improved precision by minimizing contributions from uncertain production mechanisms, making ^{36}Cl increasingly valuable for refining deglacial chronologies (Lesnek et al., 2024). We sampled glacial erratics (n = 7) and glacially polished bedrock (n = 5) located on or near the summits of six peaks throughout a 1,115 km^2 area of the High Peak Wilderness region of the ADK (Fig. 2 & 3). Samples were acquired using an angle grinder assisted by hammer and chisels with a sampling depth of ~2 cm to limit the influence of attenuation of cosmic rays thus increasing the likelihood of full nuclide production since exposure. Boulder samples were greater than 0.7 m in height, flat topped, and deposited directly on, or adjacent to, glacially polished bedrock. Sample collection was preferentially taken from areas of the boulders that did not show obvious signs of post-depositional erosion and exhibited geologic indicators of glacial polish and abrasion. These strict selection criteria were followed to limit geologic processes that could contribute to inaccurate TCN exposure ages including post-

https://doi.org/10.5194/egusphere-2026-6214
Preprint. Discussion started: 10 November 2026
© Author(s) 2026. CC BY 4.0 License.

depositional movement, erosion of accumulated nuclides, or exhumation. Latitude, longitude, and altitude for each sample were recorded using a handheld Garmin GPS with accuracy within 5-10 m. Surface inclination was measured using a Brunton compass and topographic shielding was determined in the field with an inclinometer and later calculated using the CRONUS Topographic Shielding calculator (Balco et al., 2008).

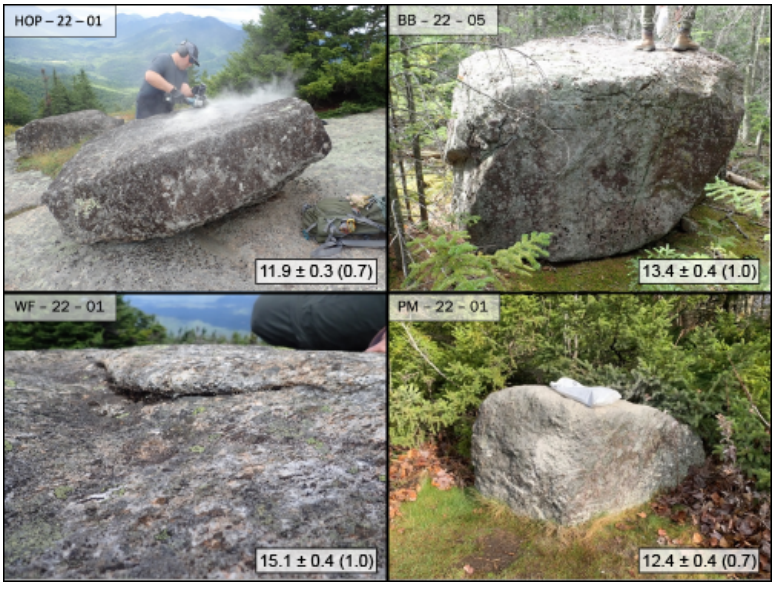


Figure 3: Boulder and bedrock samples. Examples of samples collected in this study for the purposes of ^{36}Cl surface exposure dating. Sample name is located in the top left of each frame with the associated exposure age with analytical uncertainty in the bottom right. Total uncertainty for each sample included in parentheses.

Physical preparation of samples was completed in the Cosmogenic Exposure Dating at Rowan (CEDAR) Lab at Rowan University. The top 2 cm of each sample was crushed to a 125-250 µm size fraction and ultrasonically cleaned in a 2% HNO_3 solution. Pretreated and untreated aliquots of each sample were analyzed for both major and minor elemental composition, respectively, at ALS-Global (Table S1 and S2). Chlorine extraction was completed at the Lawrence Livermore National Laboratory Center for Accelerated Mass Spectrometry (LLNL-CAMS) using a modified version of methods described in Lesnek et al. (2024). Initial prescreening of samples to determine the native chlorine concentration was completed for 8 of the samples (Table 1). One-gram aliquots were prepared in Ag(Cl, Nb) and measured for $^{35}Cl/^{37}Cl$ ratios using the low energy, pre-accelerator end of the Accelerated Mass Spectrometer (AMS) at LLNL-CAMS (Anderson et al., 2026). Native chlorine concentrations were calculated using isotopic dilution methods described in Faure & Mensing (2005). Prior to native Cl measurement, samples predicted to contain high native chlorine were magnetically separated via Frantz to isolate Ca and K- bearing feldspars. Samples yielding high native Cl concentrations (>300 ppm) were excluded from ^{36}Cl

https://doi.org/10.5194/egusphere-2026-6214
Preprint. Discussion started: 10 November 2026
© Author(s) 2026. CC BY 4.0 License.

Table 1 - Properties and analytical information for samples analyzed for cosmogenic ^{36}Cl

Location	Sample Name	Latitude (DD)	Longitude (DD)	Elevation (m)	Thickness (cm)	Density (g cm^{-3})	Shielding	Rock Dissolution (g)	^{37}Cl Carrier (g)	Cl (ppm)	$^{35/37}Cl$ (±1σ)	$^{36}Cl/Cl$ (e^{-14})	^{36}Cl conc. (e^4 at g^{-1}, ±1σ)	Exposure age (ka)
Blueberry Mountain	BB-22-02	44.2174	-73.8155	889	2	2.7	0.999	10.06	0.4015	3.6	1.1904 ± 0.0005	5.74 ± 0.24	14.31 ± 0.63	11.8 ± 0.5 (0.9)
	BB-22-05	44.2176	-73.8159	889	2	2.7	0.999	10.00	0.4019	19.5	1.1311 ± 0.0012	5.91 ± 0.14	16.43 ± 0.44	13.4 ± 0.4 (1.0)
Baxter Mountain	BXR-22-02	44.2169	-73.7653	745	2	2.7	0.999	9.97	0.4002	91.3	1.0640 ± 0.0004	6.66 ± 0.14	26.62 ± 0.62	16.9 ± 0.4 (1.6)
	BXR-22-03	44.2156	-73.7631	739	2	2.7	0.999	10.02	0.4021	296.8	1.0936 ± 0.0008	7.64 ± 0.16	57.22 ± 1.22	19.5 ± 0.5 (3.5)
	BXR-22-05	44.2156	-73.7606	715	2	2.7	0.999	5.23	0.4008	1.0	1.3253 ± 0.0005	2.35 ± 0.07	10.87 ± 0.38	9.7 ± 0.4 (0.7)
Hopkins Peak	HOP-22-01	44.1834	-73.7490	962	2	2.7	0.997	8.58	0.3994	11.4	2.3211 ± 0.0008	6.76 ± 0.16	20.50 ± 0.53	11.9 ± 0.3 (0.7)
	HOP-22-04	44.1834	-73.7483	964	2	2.7	1.000	10.03	0.4013	18.8	1.2954 ± 0.0005	7.04 ± 0.16	19.43 ± 0.50	14.1 ± 0.4 (0.8)
Lookout Mountain	LOM-22-02	44.3780	-73.8867	1242	2	2.7	0.996	10.00	0.3997	81.7	1.3200 ± 0.0010	7.86 ± 0.49	30.08 ± 1.89	13.9 ± 0.9 (1.8)
Panther Mountain	PM-23-01	44.2342	-74.3345	682	2	2.7	0.994	10.03	0.3892	7.9	2.2200 ± 0.0008	4.72 ± 0.12	11.78 ± 0.37	12.4 ± 0.4 (0.7)
	PM-23-02	44.2341	-74.3346	682	2	2.7	0.999	10.02	0.4010	15.9	2.9221 ± 0.0016	9.44 ± 0.21	25.64 ± 0.63	23.2 ± 0.6 (1.4)
Whiteface Mountain	WF-22-01	44.3679	-73.9000	1406	2	2.7	0.998	10.07	0.4012	25.5	2.3713 ± 0.0009	12.83 ± 0.25	36.86 ± 0.75	15.1 ± 0.4 (1.0)
	WF-22-03	44.3670	-73.9015	1441	2	2.7	0.994	10.02	0.3955	157.9	1.8314 ± 0.0007	17.03 ± 0.46	86.89 ± 2.39	24.5 ± 1.1 (3.5)
Lab blanks	Cl_PB1	-	-	-	-	-	-	-	0.4007	-		0.06 ± 0.01	-	-
	Cl_PB2	-	-	-	-	-	-	-	0.3982	-		0.06 ± 0.01	-	-

Sample ^{36}Cl concentrations are corrected for ^{36}Cl contributed by blanks
Ages calculated using CRONUScalc (Marrero et al., 2015) and the LSDn scaling scheme (Lifton et al., 2014) with 1σ analytical uncertainty and total uncertainty in parentheses

https://doi.org/10.5194/egusphere-2026-6214
Preprint. Discussion started: 10 November 2026
© Author(s) 2026. CC BY 4.0 License.

extraction due to a greater contribution of the thermal neutron capture production pathway on resulting exposure ages which can lead to larger exposure age uncertainty (Gosse and Phillips, 2001; Lesnek et al., 2024).

For ^{36}Cl extraction, ~10g of sample was digested in an HF-2M HNO_3 solution over 2-3 days. Removal of insoluble fluorides was completed through centrifugation. Addition of $AgNO_3$ precipitated Cl as AgCl, and precipitate was purified by redissolving with NH_4OH and adding $BaNO_3$ to remove sulfate as $BaSO_4$. After sulfates were effectively removed, the solution was reacidified through the addition of 2M HNO_3, and $AgNO_3$ to precipitate final AgCl. The final precipitate was washed repeatedly in deionized water, dried, and packed into cathodes for AMS measurement.

Ages were calculated using CRONUS-Earth web calculator (v. 2.1; http://cronus.cosmogenicnuclides.rocks/2.1/; Marrero et al., 2016), and the time- and nuclide-dependent "LSDn" scaling scheme (Lifton et al., 2014). Ages are reported here with 1σ internal uncertainty reflecting sample extraction and AMS measurement precision. Total uncertainty is included in parentheses after each sample and reflects analytical uncertainties combined with those from the various production rates (Borchers et al., 2015). We conduct sensitivity tests for surface erosion using a range of rates experienced by the samples on the order of 0.0 to 5.0 mm ka^{-1} as described in the literature (Table S3; Gillespie and Bierman, 1995). Population ages discussed later, are calculated using the total uncertainty for each sample to account for varying contributions of each production pathway on the samples as dictated by sample elemental composition (Table S1 and S2). Previously published ^{36}Cl ages from the High Peak Wilderness (Barth et al., 2019) are recalculated using the same methods discussed here for a more precise comparison.

3.1 Ice-Sheet Modelling

To support our glacial geologic interpretations of LIS deglaciation across the ADK region, we employ the Ice Sheet and Sea-level System Model (ISSM; Larour et al., 2012) to simulate transient ice-sheet evolution over this interval. The model configuration follows Cuzzone et al. (2025), which simulated steady-state LGM conditions across the northeastern United States and dynamically downscaled the model over the ADK region. Building on this framework, we simulate the deglaciation across the ADK region from the LGM through 10 ka using surface temperature and precipitation fields from the TraCE-21ka simulation (He et al., 2013) as climate forcing. The TraCE-21ka anomalies (relative to 1850 CE) are applied to the same reference climatology as in Cuzzone et al. (2025). Following Cuzzone et al. (2025), we adopt a multi-step downscaling approach. Starting from the published LGM state, we first simulate the entire LIS deglaciation. The resulting time-evolving solution is then used to prescribe boundary conditions for a regional northeastern United States model, which in turn provides boundary conditions for a high-resolution ADK model (see Fig. 1 for model domain boundary). All model physics, parameter values, domain configurations, and downscaling procedures are identical to those in Cuzzone et al. (2025). This also includes the surface mass balance scheme, basal friction formulation, ice-flow approximation, and marine margin treatment. In this study, we focus on results from the downscaled, high-resolution ADK simulations, which resolve

https://doi.org/10.5194/egusphere-2026-6214
Preprint. Discussion started: 10 November 2026
© Author(s) 2026. CC BY 4.0 License.

both the ice sheet and underlying bedrock topography at spatial resolutions ranging from ~400 m to ~30 m, allowing us to examine local controls on ice retreat and support interpretation of regional deglaciation constraints derived from geologic observations. We do not tune the model to match the reconstructed ice history; rather, the simulations provide a physically consistent transient ice-sheet evolution driven solely by prescribed climate forcing.

4 Results

4.1 ^{36}Cl surface exposure ages

Resulting ^{36}Cl exposure ages range from 9.7 ± 0.4 (0.7) to 24.5 ± 1.1 (3.5) ka (n = 12). Seven of the ages fall within a range of 11.8 ± 0.5 (0.9) ka and 15.1 ± 0.4 (1.0) ka (Table 1). Four of the remaining ages (3 bedrock and 1 boulder) range between 16.9 ± 0.4 (1.6) ka and 24.5 ± 1.1 (3.5) ka and do not overlap within 1σ internal uncertainty of the other samples. These older ages likely reflect some amount of nuclide inheritance caused by insufficient erosion of the surface material (e.g., Briner et al., 2016). Nuclide inheritance is suggested by three of those samples (BXR-22-02; BXR-22-03; PM-23-02) located below 800 m elevation where a majority of younger ages exist at or above those elevations indicating the presence of ice after the timing suggested by the older population. Similarly, we have excluded one additional age (BXR-22-05; 9.7 ± 0.4 (0.7)) which does not overlap with other ages within uncertainty and is younger than proximal radiocarbon ages constraining ice-free conditions by 12.3 ka (95% CI: 11.4-12.8 ka; Jackson, 1989). It is therefore likely BXR-22-05 experienced some amount of post-depositional geologic uncertainty such as exhumation after the deglaciation leading to an inaccurately young age. Exposure age sensitivity tests yield results with overlapping 1σ internal uncertainty from erosional rates upwards of 5.0 mm kyr^{-1} for all but the three samples interpreted as exhibiting nuclide inheritance (BXR-22-02; BXR-22-03; PM-23-02; Table S3). From these results, paired with no geologic indicators of surface erosion on the samples, we choose to report our ^{36}Cl ages with no correction for erosion.

4.2 Ice-Sheet Modelling

Between the LGM and ~14.5 ka, the ice-sheet model simulates 1.5–2.0 km of ice thickness over the High Peaks Wilderness, with the majority of rapid thinning occurring after ~14 ka (Fig. 4). To visualize the simulated ice retreat and thinning across this region, we extracted the temporally evolving ice-sheet profile along a south-to-north transect spanning the ADK (Fig. 4; see Fig. 2 for transect location). The simulated LIS margin first retreats towards the southern extent of the ADK at ~13.5 ka and exits north of the region by ~12.0 ka. The High Peaks Wilderness remains ice-covered until ~13.0 ka, after which rapid retreat and thinning ensue, with the ice sheet completely retreating from our study region by ~12.5 ka. The simulated ice margin maintains a steep surface profile throughout the retreat across the ADK's highly variable topography, suggesting that ice-surface thinning and margin retreat occur largely synchronously rather than as clearly separated phases.

Our model results indicate that deglaciation across the Adirondack region occurred rapidly, consistent with the geologic constraints suggesting ice retreat through the High Peaks Wilderness on the order of ~0.5 kyr. To isolate local topographic

https://doi.org/10.5194/egusphere-2026-6214
Preprint. Discussion started: 10 November 2026
© Author(s) 2026. CC BY 4.0 License.

effects on deglaciation timing, we first characterize the dominant regional retreat pattern by fitting a simple spatial trend to the modeled deglaciation-age field across the ADK domain (Fig. S1; Supplemental text section 1). Subtracting this regional trend from the modeled deglaciation ages yields residuals that show where the ice becomes free earlier or later than expected from large-scale retreat alone. Although simulated ice-margin retreat seems to control the overall deglaciation pattern, binning these residuals by elevation shows that the highest elevations deglaciate up to ~0.4 kyr earlier than surrounding lowlands. This indicates that local topography modestly but systematically influenced deglaciation timing, likely through earlier emergence of high terrain as the ice sheet thinned.

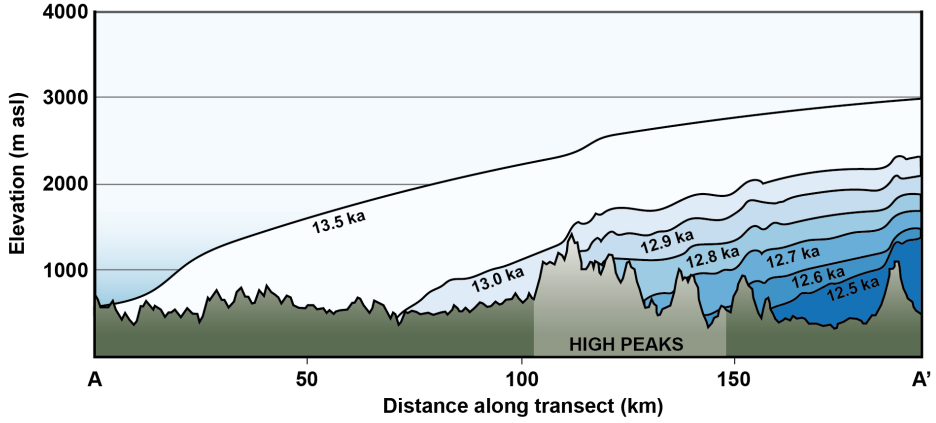


Figure 4: Transient ice sheet model profile. Simulated ice-surface elevations through time along a transect through the Adirondack Mountains between 13.5 and 12.5 ka, overlain on the bedrock topography resolved by the ice-sheet model. The location of our study area in the High Peaks is indicated by the shaded region along the transect between 100 and 150 km.

The transient simulations also provide insight into the climatic forcing associated with rapid deglaciation of the Adirondacks. The prescribed TraCE-21ka forcing (Liu et al., 2009; He et al., 2013) shows initial warming at the onset of the Bølling–Allerød (~14.7 ka), followed by brief cooling and a second, stronger warming beginning at ~13.8 ka (Fig. 5A). Despite the initial warming, most of the modeled ice-covered domain remains under positive surface mass balance, indicating that the ice sheet had begun responding to climate forcing but had not yet entered widespread ablation. During the subsequent warming at ~13.8 ka, the equilibrium-line altitude rises rapidly and approximately half of the remaining ice-covered area transitions to negative surface mass balance (Fig. 5B). Between ~13.8 and 13.2 ka, the majority of the remaining ice-covered domain experiences net ablation, and by ~13 ka nearly all remaining modeled ice is within the ablation zone. Continued ice-surface lowering during this interval likely further amplifies ablation by bringing the remaining ice surface to progressively lower elevations, contributing to rapid retreat through the High Peaks Wilderness.

https://doi.org/10.5194/egusphere-2026-6214
Preprint. Discussion started: 10 November 2026
© Author(s) 2026. CC BY 4.0 License.

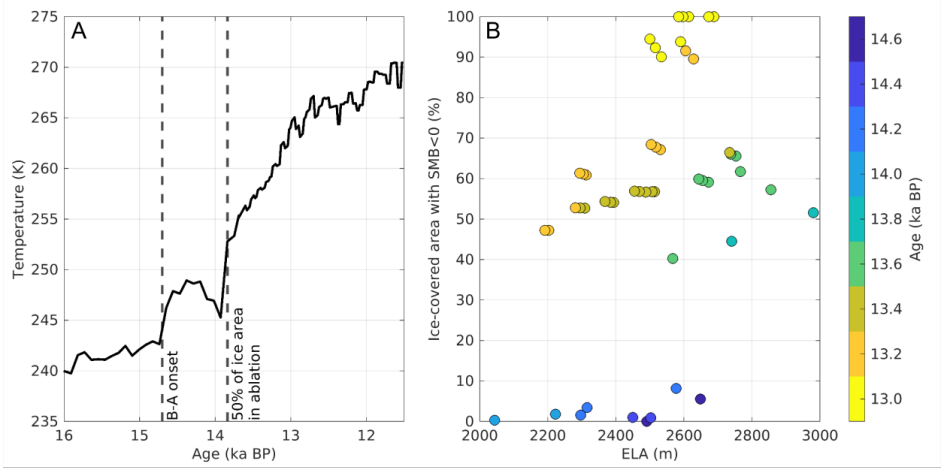


Figure 5: Model-domain-averaged transient surface temperature and simulated ablation response across the ADK region. (a) Area-averaged surface temperature from the prescribed TraCE-21ka climate forcing (Liu et al., 2009; He et al., 2013) across the ADK model domain. Dashed lines mark the canonical onset of Bølling–Allerød warming (~14.7 ka) and the time when 50% of the remaining ice-covered area in the model domain experiences negative surface mass balance. This transition approximately coincides with the onset of rapid simulated retreat across the region at ~13.8 ka. (b) Simulated equilibrium-line altitude (ELA) plotted against the fraction of the remaining ice-covered area with negative surface mass balance. Scatter points are colored by model age. The ELA is calculated from the simulated SMB = 0 contour across the ice-covered model domain. The ablation-area fraction is calculated as the area of ice-covered elements with SMB < 0 relative to the total remaining ice-covered area. The model shows a rapid expansion of the ablation area as ELA rises during the stronger warming after ~13.8 ka.

5 Discussion

5.1 Treatment of the data

Our new ^{36}Cl chronology, paired with the transient ISSM model simulations, aims to place the mechanisms and rate of exposure of LIS retreat from the High Peak Wilderness into a time context. Previous studies (Barth et al., 2019) attempted to constrain thinning of the LIS in the ADK using elevational transects of TCN exposure ages known as dipstick studies. However, the physical mechanisms presented in our new transient ISSM simulations indicate near synchronous ice thinning and margin pull back of the LIS during its final deglaciation from the region (Fig. 4). The duration of the margin retreat captured from our ice sheet simulations is shorter (~0.5 kyr) than the total uncertainty for individual ^{36}Cl ages (0.7 to 1.8 ka for non-inherited or exhumed samples), while high elevation peak exposure as nunataks occurs only ~0.2-0.4 kyr prior to margin retreat. As such, we do not differentiate between the timing of ice-sheet thinning and LIS margin retreat given the current precision of ^{36}Cl exposure data.

Barth et al. (2019) proposed that the most likely source of TCN age uncertainty at their sites was nuclide inheritance, possibly reflecting the low-erosion cold-based ice conditions that have been simulated during the LGM (Cuzzone et al., 2025). Therefore, Barth et al. (2019) interpreted the youngest age at any given elevation as the closest-limiting age for the

https://doi.org/10.5194/egusphere-2026-6214
Preprint. Discussion started: 10 November 2026
© Author(s) 2026. CC BY 4.0 License.

timing of ice-sheet thinning. Yet one of our samples (BXR-22-05) yields a ^{36}Cl age younger than the others and is interpreted to reflect post-depositional exhumation. Furthermore, although not accounted for in our reported ages, erosion can have varying effects on calculated ^{36}Cl exposure ages, making some samples appear older and others younger due to enhanced thermal neutron capture just below the surface, depending on native Cl concentration. Together, these sources of uncertainty within our TCN exposure data lower our confidence in treating any one age as more accurate than another.

Therefore, given the potential uncertainty in our individual ^{36}Cl ages and the rapid retreat of the LIS through the High Peaks Wilderness, we interpret the exposure ages as a statistical population representing the timing of ice abandonment from the region. Treating the dataset as a population accounts for variability among individual ages arising from geological processes while providing a statistically derived estimate of deglaciation. Because the same processes affecting our new ^{36}Cl ages would also have affected ages reported from Barth et al., (2019), we combine both data sets to estimate the timing of the final retreat of the LIS from the High Peak Wilderness.

5.2 Calculating the timing of deglaciation

The combined data set of 17 ^{36}Cl exposure ages from this study (n = 7) and Barth et al. (2019; n = 10, excluding outliers) are treated as a population constraining the timing of LIS deglaciation from the High Peak Wilderness of the ADK. Updated ^{36}Cl extraction methodologies (Lesnek et al., 2024) used to prescreen samples for high native Cl concentrations in samples improved the precision of these new ages (1.0 ka mean total uncertainty) from those of the previously published data set (1.8 ka mean total uncertainty) (Fig. 6). Where Barth et al., (2019) proposed the timing of LIS deglaciation broadly coincident with the Bølling-Allerød warming (~14.6 ka; Rasmussen et al., 2008), their interpretation was limited by lower precision data. Calculating the arithmetic mean and standard deviation of our combined ^{36}Cl data set (14.2 ± 1.3 ka) treats each data point equally thus giving equal influence to lower precision data on the final age. Additionally, the arithmetic mean ignores the individual uncertainty of each contributing age by only considering the age itself. In an effort to acknowledge variability within the precision of our ages we use the total uncertainty (combined analytical and production rate uncertainty) for each individual age to calculate the error-weighted mean and uncertainty thus emphasizing the higher-precision data in the final population age. This approach constrains the timing of LIS deglaciation from the High Peak Wilderness to 13.5 ± 0.6 ka (2σ) (Fig. 6).

https://doi.org/10.5194/egusphere-2026-6214
Preprint. Discussion started: 10 November 2026
© Author(s) 2026. CC BY 4.0 License.

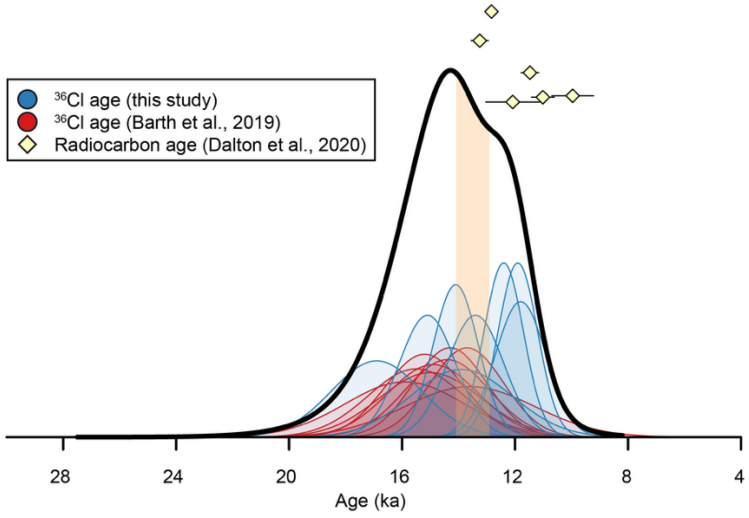


Figure 6: Exposure age probability distribution. Cumulative probability distribution of the combined ^{36}Cl exposure age data set excluded outliers shown in the bold black line. Individual age probability distributions for this study (blue) and Barth et al., 2019 (red). Proximal radiocarbon ages from Dalton et al., 2020 shown as yellow diamonds (see Figure 2 for location). The vertical orange bar represents the reported deglacial age of the High Peaks as determined from our data (13.5 ± 0.6 ka (2σ)).

This new age of deglaciation for the High Peaks Wilderness is consistent with local radiocarbon interpretations which suggest ice-free conditions by ~13.0 – 8.8 cal ka (Fig. 2, 6; Davis, 1999; Jackson et al., 1983; Noren et al., 2002). Additionally, our associated ice-sheet model simulations support this revised timing of deglaciation of the High Peak Wilderness with results suggesting deglaciation of the study region between ~13-12.5 ka.

5.3 Regional context

Significant efforts have been made to constrain the timing of ice retreat from the ADK (e.g., Barth et al., 2019; Franzi et al., 2015, 2025; Jackson, 1983; Porreca et al., 2018; Rayburn et al., 2007). Our new chronology refines the timing of deglaciation of the LIS using ^{36}Cl exposure dating methods with improved precision, constraining the timing of exposure of the High Peak Wilderness at 13.5 $\pm$ 0.6 ka (2σ). Previous large-scale reconstructions of the LIS (e.g., Dalton et al., 2020, 2023) of this precise region suggest an earlier deglacial timing (~15.0-14.0 ka). However, these reconstructions were dependent on sparse data availability, with many interpretations extrapolated from chronologies established in surrounding regions, rather than direct constraints within the High Peaks Wilderness (Fig 1, 2).

Our new chronology indicates that the High Peak Wilderness remained ice covered until later in the deglacial sequence than previously proposed (Barth et al., 2019; Dalton et al., 2020, 2023), thus refining the timing of LIS retreat as a response to the onset of Bølling-Allerød warming. This interpretation is supported by regional paleo-lake formation and routing evidence from the ADK and surrounding areas. LIS presence in the ADK forced a subdued Lake Iroquois to drain eastward through

https://doi.org/10.5194/egusphere-2026-6214
Preprint. Discussion started: 10 November 2026
© Author(s) 2026. CC BY 4.0 License.

the Glaciomohawk River to the south of the High Peaks Wilderness (Fairchild, 1912; Franzi et al., 2025; Pair and Rodrigues, 1993) where ^{10}Be exposure ages from strath terraces suggest opening of the meltwater routing pathway 14.7 ± 1.3 ka (Porreca et al., 2016). Strandline deposits and beach ridges along the western edge of the ADK indicate northward expansion of Lake Iroquois coincident with northward retreat of the LIS (Franzi et al., 2025). Drainage of the glacial lake through the Covey Hill channel north of the ADK is proposed to have occurred ~13 ka therefore acting as a minimum-limiting age for the deglaciation of the High Peaks 13.5 ± 0.6 ka. Combined, the paleo-lake strandlines, strath terrace exposure ages, transient model simulation, and High Peaks Wilderness TCN data suggest a consistent sequence of ADK deglaciation where retreat of the LIS margin 14.7 ± 1.3 ka opened the Glaciomohawk River outlet for Lake Iroquois, followed by ice retreating through the ADK ~14.0-12.5 ka with the High Peaks becoming exposed 13.5 ± 0.6 ka, and the Covey Hill outlet opening ~13 ka allowing drainage of the glacial lake down the Champlain River Valley. Additionally, these data indicate that the High Peak Wilderness of the ADK remained uncovered throughout the Younger Dryas, when there was proposed stabilization of the ice sheet north of Covey Hill (Franzi et al., 2025).

Broadening the regional context, ^{10}Be ages from two moraines in New Hampshire and Maine, the Littleton-Bethlehem (13.2 ± 0.8 ka total uncertainty) and Androscoggin (13.8 ± 0.7 ka total uncertainty) moraines (Fig. 1), are statistically indistinguishable from our High Peaks Wilderness deglacial age (Bromley et al., 2015). Collectively, these ages might point towards a regional LIS response to inter-Allerød warming, with stabilization of the ice sheet leading to moraine development followed by retreat occurring ~13.5 ka. Previously published interpretations suggest that the LIS began to retreat in the ADK at the onset of Bølling-Allerød warming (Barth et al., 2019). However, the chronologies presented here indicate a later timing of deglaciation, occurring within the Allerød warm interval.

The transient ice-sheet simulations provide physical context for the revised chronology. In the model, the initial Bølling–Allerød warming at ~14.7 ka does not immediately produce widespread ablation across the Adirondacks. Instead, widespread negative surface mass balance develops during the stronger warming beginning at ~13.8 ka, when the equilibrium-line altitude rises rapidly and a large fraction of the remaining ice-covered area enters the ablation zone (Fig. 5; Supplemental text section 2). This two-step structure reflects the prescribed TraCE-21ka climate forcing (Liu et al., 2009; He et al., 2013) and should not be interpreted as a direct reconstruction of local Adirondack temperature history. However, regional paleoclimate records from the southern Great Lakes indicate that Bølling–Allerød warming in the continental interior may have occurred several centuries later than in mid-latitude Northern Hemisphere syntheses, with accelerated warming centered near ~14 ka (Watson et al., 2018). Continued thinning and retreat in the model then lead to rapid deglaciation of the High Peaks Wilderness. The apparent lag between the onset of Bølling–Allerød warming and complete exposure of the High Peaks Wilderness therefore likely reflects the time required to remove a thick interior ice mass, rather than a delayed onset of ice-sheet response to climate forcing.

https://doi.org/10.5194/egusphere-2026-6214
Preprint. Discussion started: 10 November 2026
© Author(s) 2026. CC BY 4.0 License.

6 Conclusions

New ^{36}Cl exposure ages from numerous summits throughout the High Peak Wilderness region of the Adirondack Mountains of New York have been used to calculate the age of deglaciation of the LIS from the region. These new data are paired with transient ice-sheet model simulations of LIS deglaciation, which indicate rapid retreat through the study area over an approximately 500-year interval. Simulated deglaciation is dominated by rapid regional ice-margin retreat, although ice-sheet thinning allows the highest peaks to emerge as nunataks ~0.2-0.4 kyr before surrounding low-elevation terrain. This difference is finer than the resolution of the available TCN exposure ages. Combining the new exposure ages with previously published ages from the High Peaks Wilderness (Barth et al., 2019) yields a deglaciation age of 13.5 ± 0.6 ka (2σ), indicating a later timing of deglaciation of the central Adirondacks than proposed in transgressive reconstructions of the ice sheet. Together with the model results, these data support rapid LIS retreat through the region, but place this retreat later in the deglaciation than previously thought. The persistence of thick ice over the ADK later into the deglaciation therefore has implications for the broader timing and response of the LIS to abrupt warming events such as the Bølling-Allerød.

Code and data availability

All data needed to evaluate the manuscript including geochemical data and sensitivity tests are presented in the text or Supplemental Information. The Ice-sheet and Sea-level System Model (ISSM) is publicly available at https://github.com/ISSMteam/ISSM. The model configurations, transient simulation outputs, and MATLAB analysis scripts used in this study are available through Zenodo at https://doi.org/10.5281/zenodo.23932502.

Supplement link

The link to the supplement will be included by Copernicus, if applicable.

Author contributions

KB: methodology, investigation, formal analysis, visualization, writing – original draft, writing – reviewing and editing.
AMB: conceptualization, methodology, investigation, formal analysis, funding acquisition, writing – reviewing and editing.
JKC: conceptualization, methodology, investigation, formal analysis, funding acquisition, writing – reviewing and editing.
AH: investigation, formal analysis, writing - reviewing and editing.

Competing interests

The authors declare they have no competing interests.

https://doi.org/10.5194/egusphere-2026-6214
Preprint. Discussion started: 10 November 2026
© Author(s) 2026. CC BY 4.0 License.

Disclaimer

Copernicus Publications adds a standard disclaimer: "Copernicus Publications remains neutral with regard to jurisdictional claims made in the text, published maps, institutional affiliations, or any other geographical representation in this paper. While Copernicus Publications makes every effort to include appropriate place names, the final responsibility lies with the authors. Views expressed in the text are those of the authors and do not necessarily reflect the views of the publisher." Please feel free to add disclaimer text at your choice, if applicable.

Acknowledgements

The authors acknowledge field and lab assistance from Kirsten Hill, Lauren Schneider, Mallory Osmun, Nicholas Giannini, Lou Morgan, and Dylan Ayars.

Financial support

KB, AMB, and JKC disclose support for this research from the National Science Foundation (grant number 2133698). KB and AMB disclose additional support for the research and publication of this work from Rowan University.

References

Anderson, Tyler S., and Alan Hidy. *Technical Note: Stable Chloride Measurements at Cams*, 27 July 2026, https://doi.org/10.5194/egusphere-2026-4091.

Ashwal, L.D., 1993. Anorthosites, Minerals, Rocks and Mountains. Springer-Berlag, New York, NY. http://dx.doi.org/10.1007/978-3-642-77440-9

Balco, G., Schaefer, J., 2006. Cosmogenic-nuclide and varve chronologies for the deglaciation of southern New England. Quaternary Geochronology 1, 15–28. https://doi.org/10.1016/j.quageo.2006.06.014

Balco, G., Stone, J.O., Lifton, N.A., Dunai, T.J., 2008. A complete and easily accessible means of calculating surface exposure ages or erosion rates from 10Be and 26Al measurements. Quaternary Geochronology 3, 174–195. https://doi.org/10.1016/j.quageo.2007.12.001

Balter-Kennedy, A., Schaefer, J.M., Balco, G., Kelly, M.A., Kaplan, M.R., Schwartz, R., Oakley, B., Young, N.E., Hanley, J., Varuolo-Clarke, A.M., 2024. The Laurentide Ice Sheet in southern New England and New York during and at the end of the Last Glacial Maximum: a cosmogenic-nuclide chronology. Clim. Past. https://doi.org/10.5194/cp-20-2167-2024

Barth, A.M., Marcott, S.A., Licciardi, J.M., Shakun, J.D., 2019. Deglacial Thinning of the Laurentide Ice Sheet in the Adirondack Mountains, New York, USA, Revealed by ^{36}Cl Exposure Dating. Paleoceanography and Paleoclimatology 34, 946–953. https://doi.org/10.1029/2018PA003477

Borchers, B., Marrero, S., Balco, G., Caffee, M., Goehring, B., Lifton, N., Nishiizumi, K., Phillips, F., Schaefer, J., Stone, J., 2015. Geological calibration of spallation production rates in the CRONUS-Earth project. Quaternary Geochronology 31, 188–198. https://doi.org/10.1016/j.quageo.2015.01.009

Bromley, G.R., Hall, B.L., Thompson, W.B., Kaplan, M.R., Garcia, J.L., Schaefer, J.M., 2015. Later glacial fluctuations of the Laurentide Ice Sheet in the White Mountains of Maine and New Hampshire, U.S.A. Quaternary Research 83, 522–530. https://doi.org/10.1016/j.yqres.2015.02.004

Clark, P.U., Dyke, A.S., Shakun, J.D., Carlson, A.E., Clark, J., Wohlfarth, B., Mitrovica, J.X., Hostetler, S.W., McCabe, A.M., 2009. The Last Glacial Maximum. Science 325, 710–4. https://doi.org/10.1126/science.1172873

Clark, P.U., Pisias, N.G., Stocker, T.F., Weaver, A.J., 2002. The role of the thermohaline circulation in abrupt climate change. Nature 415, 863–869. DOI:10.1038/415863a

https://doi.org/10.5194/egusphere-2026-6214
Preprint. Discussion started: 10 November 2026
© Author(s) 2026. CC BY 4.0 License.



Corbett, L.B., Bierman, P.R., Stone, B.D., Caffee, M.W., Larsen, P.L., 2017. Cosmogenic nuclide age estimate for Laurentide Ice Sheet recession from the terminal moraine, New Jersey, USA, and constraints on latest Pleistocene ice sheet history. Quaternary Research 87, 482–498. https://doi.org/10.1017/qua.2017.11

Cuzzone, J.K., Barth, A., Barker, K., Morlighem, M., 2025. Ice sheet model simulations reveal that polythermal ice conditions existed across the northeastern USA during the Last Glacial Maximum. The Cryosphere 19, 1559–1575. https://doi.org/10.5194/tc-19-1559-2025

Dalton, A.S., Dulfer, H.E., Margold, M., Heyman, J., Clague, J.J., Froese, D.G., Gauthier, M.S., Hughes, A.L.C., Jennings, C.E., Norris, S.L., Stoker, B.J., 2023. Deglaciation of the north American ice sheet complex in calendar years based on a comprehensive database of chronological data: NADI-1. Quaternary Science Reviews 321, 108345. https://doi.org/10.1016/j.quascirev.2023.108345

Dalton, A.S., Margold, M., Stokes, C.R., Tarasov, L., Dyke, A.S., Adams, R.S., Allard, S., Arends, H.E., Atkinson, N., Attig, J.W., Barnett, P.J., Barnett, R.L., Batterson, M., Bernatchez, P., Borns, H.W., Breckenridge, A., Briner, J.P., Brouard, E., Campbell, J.E., Carlson, A.E., Clague, J.J., Curry, B.B., Daigneault, R.-A., Dubé-Loubert, H., Easterbrook, D.J., Franzi, D.A., Friedrich, H.G., Funder, S., Gauthier, M.S., Gowan, A.S., Harris, K.L., Hétu, B., Hooyer, T.S., Jennings, C.E., Johnson, M.D., Kehew, A.E., Kelley, S.E., Kerr, D., King, E.L., Kjeldsen, K.K., Knaeble, A.R., Lajeunesse, P., Lakeman, T.R., Lamothe, M., Larson, P., Lavoie, M., Loope, H.M., Lowell, T.V., Lusardi, B.A., Manz, L., McMartin, I., Nixon, F.C., Occhietti, S., Parkhill, M.A., Piper, D.J.W., Pronk, A.G., Richard, P.J.H., Ridge, J.C., Ross, M., Roy, M., Seaman, A., Shaw, J., Stea, R.R., Teller, J.T., Thompson, W.B., Thorleifson, L.H., Utting, D.J., Veillette, J.J., Ward, B.C., Weddle, T.K., Wright, H.E., 2020. An updated radiocarbon-based ice margin chronology for the last deglaciation of the North American Ice Sheet Complex. Quaternary Science Reviews 234, 106223. https://doi.org/10.1016/j.quascirev.2020.106223

Davis, P.T., 1999. Cirques of the Presidential Range, New Hampshire, and surrounding alpine areas in the northeastern United States. Geographie physique et Quaternaire 53, 25–45. DOI: 10.7202/004784ar

Dyke, A.S., 2004. An outline of North American Deglaciation with emphasis on central and northern Canada 371–406. DOI:10.1016/S1571-0866(04)80209-4

Fairchild, H.L., 1913. Pleistocene Geology of New York State. I. Science 37, 237–249. https://doi.org/10.1126/science.37.946.237

Faure, G. and Mensing, T. M.: Isotopes: Principles and Applications, Third edition., John Wiley and Sons, Hoboken, New Jersey, 2005. ISBN: 978-0-471-38437-3

Franzi, D.A., Carl, B.S., Pepperstone, H.S., 2026. Late glacial lake and marine strandlines in the Ontario, St. Lawrence, and Champlain Lowlands, USA and Canada record steadily decreasing water levels interrupted by breakout floods. Quat. res. 129, 1–18. https://doi.org/10.1017/qua.2025.15

Franzi, David A.; Ridge, John C.; Pair, Donald L.; Desimone, David; Rayburn, John A.; and Barclay, David J. (2016) "Post-Valley Heads Deglacation of the Adirondack Mountains and Adjacent Lowlands," Adirondack Journal of Environmental Studies: Vol. 21: No. 1, Article 11.Available at: https://digitalworks.union.edu/ajes/vol21/iss1/11

Gillespie, A.R., Bierman, P.R., 1995. Precision of terrestrial exposure ages and erosion rates estimated from analysis of cosmogenic isotopes produced in situ. J. Geophys. Res. 100, 24637–24649. https://doi.org/10.1029/95JB02911

Gosse, J.C., Phillips, F.M., 2001. Terrestrial in situ cosmogenic nuclides: theory and application. Quaternary Science Reviews 20, 1475–1560. DOI: 10.1016/S0277-3791(00)00171-2

He, F., Shakun, J.D., Clark, P.U., Carlson, A.E., Liu, Z., Otto-Bliesner, B.L., Kutzbach, J.E., 2013. Northern Hemisphere forcing of Southern Hemisphere climate during the last deglaciation. Nature 494, 81–5. https://doi.org/10.1038/nature11822

Isachsen, Y. W., Fisher, D. W., & Rickard, L. V. (1970). *Geologic map of New York State: Adirondack sheet* (Map and Chart Series No. 15) [Map]. New York State Museum and Science Service. usgs.gov

Isachsen, Yngvar W. "Contemporary doming of the Adirondack Mountains: Further evidence from releveling." *Tectonophysics*, vol. 71, no. 1–4, Jan. 1981, pp. 95–96, https://doi.org/10.1016/0040-1951(81)90051-2.

Jackson, S.T., 1989. Postglacial Vegetational Changes Along an Elevational Gradient in the Adirondack Mountains (New York), Bulletin / New York State Museum. University of the State of New York, State Education Dept., New York State Museum, Biological Survey, Albany, NY. DOI: 10.5962/bhl.title.135549

https://doi.org/10.5194/egusphere-2026-6214
Preprint. Discussion started: 10 November 2026
© Author(s) 2026. CC BY 4.0 License.

Larour, E., et al. “Continental scale, high order, high spatial resolution, Ice Sheet modeling using the Ice Sheet System Model (ISSM).” *Journal of Geophysical Research: Earth Surface*, vol. 117, no. F1, Mar. 2012, https://doi.org/10.1029/2011jf002140.

Lesnek, A.J., Licciardi, J.M., Hidy, A.J., Anderson, T.S., 2024. Technical note: Optimizing the in situ cosmogenic ^{36}Cl extraction and measurement workflow for geologic applications. Geochronology 6, 475–489. https://doi.org/10.5194/gchron-6-475-2024

Licciardi, J.M., Teller, J.T., Clark, P.U., 1999. Freshwater routing by the Laurentide Ice Sheet during the last deglaciation, in: Clark, U., Webb, S., Keigwin, D. (Eds.), Geophysical Monograph Series. American Geophysical Union, Washington, D. C., pp. 177–201. https://doi.org/10.1029/GM112p0177

Lifton, N., Sato, T., Dunai, T.J., 2014. Scaling in situ cosmogenic nuclide production rates using analytical approximations to atmospheric cosmic-ray fluxes. Earth and Planetary Science Letters 386, 149–160. https://doi.org/10.1016/j.epsl.2013.10.052

Liu, Z., Otto-Bliesner, B.L., He, F., Brady, E.C., Tomas, R., Clark, P.U., Carlson, A.E., Lynch-Stieglitz, J., Curry, W., Brook, E., Erickson, D., Jacob, R., Kutzbach, J., Cheng, J., 2009. Transient simulation of last deglaciation with a new mechanism for Bølling-Allerød warming. Science 325, no. 5938, pp. 310-314.

Marrero, S.M., Phillips, F.M., Borchers, B., Lifton, N., Aumer, R., Balco, G., 2015. Cosmogenic nuclide systematics and the CRONUScalc program. Quaternary Geochronology 31, 160–187. https://doi.org/10.1016/j.quageo.2015.09.005

Noren, A.J., Bierman, P.R., Steig, E.J., Lini, A., Southon, J., 2002. Millennial-scale storminess variability in the northeastern United States during the Holocene epoch. Nature 419, 821–824. https://doi.org/10.1038/nature01132

Pair, D.L., Rodrigues, C.G., 1993. Late Quaternary Deglaciation of the Southwest St. Lawrence Lowland, New York and Ontario. Geological Society of America Bullitin, 105: pp.1151-1164. DOI:10.1139/E05-118

Porreca, C., Briner, J.P., Kozlowski, A., 2018. Laurentide ice sheet meltwater routing along the Iro-Mohawk River, eastern New York, USA. Geomorphology 303, 155–161. https://doi.org/10.1016/j.geomorph.2017.12.001

Rasmussen, S.O., Seierstad, I.K., Andersen, K.K., Bigler, M., Dahl-Jensen, D., Johnsen, S.J., 2008. Synchronization of the NGRIP, GRIP, and GISP2 ice cores across MIS 2 and palaeoclimatic implications. Quaternary Science Reviews 27, 18–28. https://doi.org/10.1016/j.quascirev.2007.01.016

Rayburn, J.A., Franzi, D.A., Knuepfer, P.L.K., 2007. Evidence from the Lake Champlain Valley for a later onset of the Champlain Sea and implications for late glacial meltwater routing to the North Atlantic. Palaeogeography, Palaeoclimatology, Palaeoecology 246, 62–74. https://doi.org/10.1016/j.palaeo.2006.10.027

Ridge, J.C., Balco, G., Bayless, R.L., Beck, C.C., Carter, L.B., Dean, J.L., Voytek, E.B., Wei, J.H., 2012. The New North American Varve Chronology: A Precise Record of Southeastern Laurentide Ice Sheet Deglaciation and Climate, 18.2-12.5 kyr BP, and Correlations with Greenland Ice Core Records. American Journal of Science 312, 685–722. https://doi.org/10.2475/07.2012.01%5D

Stanford, S.D., 2010. Onshore record of Hudson River drainage to the continental shelf from the late Miocene through the late Wisconsinan deglaciation, USA: synthesis and revision. Boreas 39, 1–17. https://doi.org/10.1111/j.1502-3885.2009.00106.x

Thompson, W. B., Dorion, C. C., Ridge, J. C., Balco, G., Fowler, B. K., & Svendsen, K. M. (2017). Deglaciation and late-glacial climate change in the White Mountains, New Hampshire, USA. *Quaternary Research*, *87*(1), 96–120. doi:10.1017/qua.2016.4

Watson, Benjamin I., et al. “Temperature variations in the southern Great Lakes during the last deglaciation: Comparison between pollen and GDGT proxies.” *Quaternary Science Reviews*, vol. 182, Feb. 2018, pp. 78–92, https://doi.org/10.1016/j.quascirev.2017.12.011.